JCI The Journal of Clinical Investigation

Cardiac mast cells cause atrial fibrillation through PDGF-A–mediated fibrosis in pressure-overloaded mouse hearts

Chien-hui Liao, Hiroshi Akazawa, Masaji Tamagawa, Kaoru Ito, Noritaka Yasuda, Yoko Kudo, Rie Yamamoto, Yukako Ozasa, Masanori Fujimoto, Ping Wang, Hiromitsu Nakauchi, Haruaki Nakaya, Issei Komuro

J Clin Invest. 2010;120(1):242-253. https://doi.org/10.1172/JCI39942.

Research Article **Cardiology**

Atrial fibrillation (AF) is a common arrhythmia that increases the risk of stroke and heart failure. Here, we have shown that mast cells, key mediators of allergic and immune responses, are critically involved in AF pathogenesis in stressed mouse hearts. Pressure overload induced mast cell infiltration and fibrosis in the atrium and enhanced AF susceptibility following atrial burst stimulation. Both atrial fibrosis and AF inducibility were attenuated by stabilization of mast cells with cromolyn and by BM reconstitution from mast cell–deficient WBB6F1-*Kit*$^{W/W\text{-}v}$ mice. When cocultured with cardiac myocytes or fibroblasts, BM-derived mouse mast cells increased platelet-derived growth factor A (PDGF-A) synthesis and promoted cell proliferation and collagen expression in cardiac fibroblasts. These changes were abolished by treatment with a neutralizing antibody specific for PDGF α-receptor (PDGFR-α). Consistent with these data, upregulation of atrial *Pdgfa* expression in pressure-overloaded hearts was suppressed by BM reconstitution from WBB6F1-*Kit*$^{W/W\text{-}v}$ mice. Furthermore, injection of the neutralizing PDGFR-α–specific antibody attenuated atrial fibrosis and AF inducibility in pressure-overloaded hearts, whereas administration of homodimer of PDGF-A (PDGF-AA) promoted atrial fibrosis and enhanced AF susceptibility in normal hearts. Our results suggest a crucial role for mast cells in AF and highlight a potential application of controlling the mast cell/PDGF-A axis to achieve upstream prevention of AF in stressed hearts.

Cardiac mast cells cause atrial fibrillation through PDGF-A–mediated fibrosis in pressure-overloaded mouse hearts

Chien-hui Liao,[1,2] Hiroshi Akazawa,[1] Masaji Tamagawa,[3] Kaoru Ito,[1] Noritaka Yasuda,[1] Yoko Kudo,[1] Rie Yamamoto,[1] Yukako Ozasa,[1] Masanori Fujimoto,[1] Ping Wang,[1] Hiromitsu Nakauchi,[2] Haruaki Nakaya,[3] and Issei Komuro[1]

[1]Department of Cardiovascular Science and Medicine, Chiba University Graduate School of Medicine, Chiba, Japan. [2]Division of Stem Cell Therapy, Center for Stem Cell and Regenerative Medicine, Institute of Medical Science, University of Tokyo, Tokyo, Japan. [3]Department of Pharmacology, Chiba University Graduate School of Medicine, Chiba, Japan.

Atrial fibrillation (AF) is a common arrhythmia that increases the risk of stroke and heart failure. Here, we have shown that mast cells, key mediators of allergic and immune responses, are critically involved in AF pathogenesis in stressed mouse hearts. Pressure overload induced mast cell infiltration and fibrosis in the atrium and enhanced AF susceptibility following atrial burst stimulation. Both atrial fibrosis and AF inducibility were attenuated by stabilization of mast cells with cromolyn and by BM reconstitution from mast cell–deficient WBB6F1-*Kit*$^{W/W\text{-}v}$ mice. When cocultured with cardiac myocytes or fibroblasts, BM-derived mouse mast cells increased platelet-derived growth factor A (PDGF-A) synthesis and promoted cell proliferation and collagen expression in cardiac fibroblasts. These changes were abolished by treatment with a neutralizing antibody specific for PDGF α-receptor (PDGFR-α). Consistent with these data, upregulation of atrial *Pdgfa* expression in pressure-overloaded hearts was suppressed by BM reconstitution from WBB6F1-*Kit*$^{W/W\text{-}v}$ mice. Furthermore, injection of the neutralizing PDGFR-α–specific antibody attenuated atrial fibrosis and AF inducibility in pressure-overloaded hearts, whereas administration of homodimer of PDGF-A (PDGF-AA) promoted atrial fibrosis and enhanced AF susceptibility in normal hearts. Our results suggest a crucial role for mast cells in AF and highlight a potential application of controlling the mast cell/PDGF-A axis to achieve upstream prevention of AF in stressed hearts.

Introduction

Atrial fibrillation (AF) is a supraventricular arrhythmia that is characterized by rapid and fibrillatory atrial activation with an irregular ventricular response. AF remains the most common arrhythmia encountered in clinical practice and is associated with an increased risk of stroke, heart failure, and overall mortality (1). Several cardiovascular disorders predispose to AF, such as coronary artery disease, valvular heart disease, congestive heart failure, and hypertension, especially when LV hypertrophy is present (1). Recent electrophysiological evidence has indicated that the triggering ectopic foci act on predisposing substrates to initiate single- or multiple-circuit reentry, leading to AF (2). The most important histopathological change in AF is atrial fibrosis (3, 4). Accumulation of ECM proteins has been documented in biopsied specimens of atrium from patients with AF (5), and experimental studies using animal models have indicated that interstitial deposition of dense ECM proteins causes separation between bundles of atrial myocytes and disturbs cell-to-cell impulse propagation (3, 4). In addition, atrial fibrosis potentially exaggerates myocardial ischemia by hampering oxygen diffusion and alters the electrophysical and biomechanical properties of atrial myocytes, allowing the initiation and perpetuation of AF (4). The mechanisms underlying the development of atrial fibrosis in AF remain unclear, but evolving evidence has suggested that inflammation is profoundly implicated in the process of the structural remodeling in the atrium (4, 6). Inflammatory infiltrates were observed in the atrium of AF patients and animal models (7, 8). Furthermore, inflammatory biomarkers such as C-reactive protein were elevated in AF patients and were associated with the presence of AF and the future development of AF (9, 10). However, it remains to be fully elucidated how inflammation is linked to the development of structural remodeling as a susceptible AF substrate in stressed hearts.

Mast cells function as key effector cells during allergic and immune responses through releasing preformed or newly synthesized bioactive products (11). Recent studies have implicated mast cells in inflammation and tissue remodeling (11, 12). Indeed, mast cells reside in many tissues including the heart (13) and participate in the inflammatory process underlying several cardiovascular disorders, such as atherosclerosis (14, 15), aortic aneurysm (16, 17), heart failure (18), viral myocarditis (19), and ventricular arrhythmia during ischemia/reperfusion injury (20). In particular, mast cell–derived IL-6 and IFN-γ have been reported to promote atherosclerosis and abdominal aortic aneurysm (15, 16). Meanwhile, mast cells enhance the fibrogenic process through the release of multiple proteases and inflammatory cytokines in the skin, lung, and kidney (21–24). Here, we demonstrate that mast cells infiltrate the atrium of pressure-overloaded mice and contribute to the pathogenesis of atrial fibrosis and AF susceptibility. Mechanistically, upregulation of PDGF-A mediates the fibrogenic effect of mast cells in promoting AF. These results provide mechanistic insights into the pathogenic role of mast cells in promoting an AF substrate in stressed hearts.

Conflict of interest: The authors have declared that no conflict of interest exists.
Citation for this article: *J. Clin. Invest.* **120**:242–253 (2010). doi:10.1172/JCI39942.

Table 1
Echocardiographic measurements in TAC- and sham-operated mice with or without treatment with cromolyn

	Sham		TAC	
Cromolyn	(–)	(+)	(–)	(+)
Number	10	5	17	15
HW/BW (mg/g)	4.55 ± 0.11	4.64 ± 0.04	5.24 ± 0.05[A]	5.54 ± 0.13[A]
HR (bpm)	610.10 ± 7.59	613.20 ± 3.44	599.24 ± 7.30	622.67 ± 7.05
LVDd (mm)	3.58 ± 0.08	3.51 ± 0.08	3.55 ± 0.04	3.54 ± 0.09
LVDs (mm)	1.99 ± 0.06	2.06 ± 0.05	2.05 ± 0.04	1.97 ± 0.07
FS (%)	44.5 ± 0.87	41.2 ± 0.99	42.2 ± 0.62	44.6 ± 0.91
LVPWth (mm)	0.65 ± 0.11	0.64 ± 0.04	0.81 ± 0.01[A]	0.82 ± 0.01[A]

[A]$P < 0.01$ versus sham. FS, fractional shortening; HR, heart rate; HW/BW, heart-to-body weight ratio; LVDd, LV diameter in end diastole; LVDs, LV diameter in end systole; LVPWth, LV posterior wall thickness in end diastole.

Results

Atrial burst stimulation induces AF in pressure-overloaded hearts. To develop a model of AF associated with LV hypertrophy, we first induced pressure overload in mice by producing transverse aorta constriction (TAC) (25). On day 10, TAC-operated mice showed a significant increase in heart–to–body weight and LV wall thickness with preserved fractional shortening (Table 1). The atrium–to–body weight ratios were increased 36%, from 0.22 ± 0.02 mg/g in sham-operated mice ($n = 5$) to 0.30 ± 0.02 mg/g in TAC-operated mice ($n = 5$; $P < 0.01$), indicating that TAC operation induced hemodynamic overload in both the atrium and ventricle. We recorded ECGs using telemetry at 10 days after the operation, but no episode of spontaneous AF was observed in TAC- or sham-operated mice (Supplemental Figure 1; supplemental material available online with this article; doi:10.1172/JCI39942DS1).

To test the inducibility of AF, we applied programmed electrical stimulation directly to right atrium under Langendorff perfusion at 10 days after the operation. During the period for stabilization prior to stimulation, spontaneous episodes of AF were not observed in TAC- or sham-operated hearts. However, the induction of AF was attainable and reliably reproducible with programmed electrical stimulation of right atrium (Figure 1A). AF was defined as an episode of rapid and chaotic atrial rhythm and irregular ventricular response. AF was induced more frequently in TAC-operated hearts (100%) than in sham-operated hearts (20%) (Figure 1, A–C). In addition, the duration of AF episodes in TAC-operated hearts was significantly longer than that in sham-operated hearts (Figure 1D). We also applied atrial stimulation under Langendorff perfusion at 28 days after TAC operation. However, TAC-operated hearts showed severe LV dysfunction (fractional shortening, 16.6% ± 8.4%) at this time point, and undesirable arrhythmias such as ventricular fibrillation were induced each time after stimulation, which hampered our evaluation of AF arrhythmogenesis. Therefore, atrial burst stimulation under Langendorff perfusion at 10 days after TAC operation represents a valid ex vivo model that permits study of AF substrate, especially in the setting of LV hypertrophy.

Mast cells are accumulated and activated in the atrium of TAC-operated mice. To assess the contribution of mast cells to atrial arrhythmogenicity, we evaluated the contents of mast cells in atrium by staining histological sections with toluidine blue. The number of infiltrating mast cells showed a 2.5-fold increase in TAC-operated mice on day 10, as compared with sham-operated mice (Figure 2A). Avidin conjugated to fluorochrome dyes binds to the negatively charged heparin proteoglycans and identifies the granules of mast cells (20, 26). In the left and right atria of TAC-operated mice, we observed a marked increase of mast cell activation with the presence of extruded avidin-positive granules close to cell surface (Figure 2B). These results suggest that mast cells are accumulated and activated in the atrium of pressure-overloaded hearts.

Stabilization of mast cells by cromolyn attenuates AF in TAC-operated hearts. Accumulation of mast cells in the atrium indicated a causal link between infiltration of these cells and the pathogenesis of AF. To determine the importance of mast cells in this process, we systemically administered the mast cell stabilizer cromolyn (14, 20) to TAC-operated mice. In the atrium at 10 days after TAC operation, the degranulation of mast cells was almost completely inhibited by cromolyn treatment (Figure 2B), although the mast cell contents were not significantly decreased ($P = 0.17$; Figure 2A). Echocardiographic parameters regarding LV hypertrophy and systolic function remained unchanged by cromolyn treatment (Table 1). As revealed by histology, there was no significant difference in the average size of ventricular myocytes between cromolyn- and vehicle-treated mice (Supplemental Figure 2). In addition, the atrium–to–body weight ratios at 10 days after TAC operation were not significantly different between cromolyn- and vehicle-treated mice (0.30 ± 0.02 mg/g vs. 0.28 ± 0.02 mg/g; $P = 0.43$). These results suggest that cromolyn did not affect the hemodynamic workload. However, as compared with vehicle-treated mice, cromolyn-treated mice showed a remarkable reduction in the incidence and duration of AF episodes after atrial burst stimulation under Langendorff perfusion (Figure 3, A–C). To validate and extend our ex vivo findings, we subjected anesthetized mice to rapid transesophageal atrial pacing and simultaneous surface ECG recording at 10 days after the operation. AF could be induced in vivo after atrial burst stimulation in TAC-operated mice, but not in sham-operated mice (Figure 3, D–F). Similarly, cromolyn treatment completely suppressed AF induced by transesophageal atrial pacing in TAC-operated mice (Figure 3, G and H).

Atrial fibrosis is a major feature of structural remodeling that contributes to AF substrate (3, 4). In the atrium of TAC-operated mice, Masson's trichrome staining revealed areas of interstitial fibrosis (Figure 3I), and hydroxyproline assay indicated deposition of collagen (Figure 3J). Mast cell stabilization by cromolyn remarkably attenuated fibrotic changes in the atrium of TAC-operated mice (Figure 3, I and J). These results suggest that stabilization of mast cells prevents atrial structural remodeling and AF inducibility in TAC-operated mice.

Reconstitution with BM cells from mast cell–deficient W/W^v mice attenuates AF in TAC-operated hearts. To further examine the role of mast cells in AF, we utilized mast cell–deficient *WBB6F1-Kit$^{W/W\text{-}v}$* (W/W^v) mice carrying compound heterozygous mutations of *c-kit* (*Kit^W*, null; *Kit$^{W\text{-}v}$*, dominant negative). To circumvent the undesirable effects by altered c-kit signaling in nonhematopoietic cells, we reconstituted C57BL/6 mice with BM cells from W/W^v mice or control *WBB6F1-Kit$^{+/+}$* (+/+) mice. We first confirmed, by tolu-

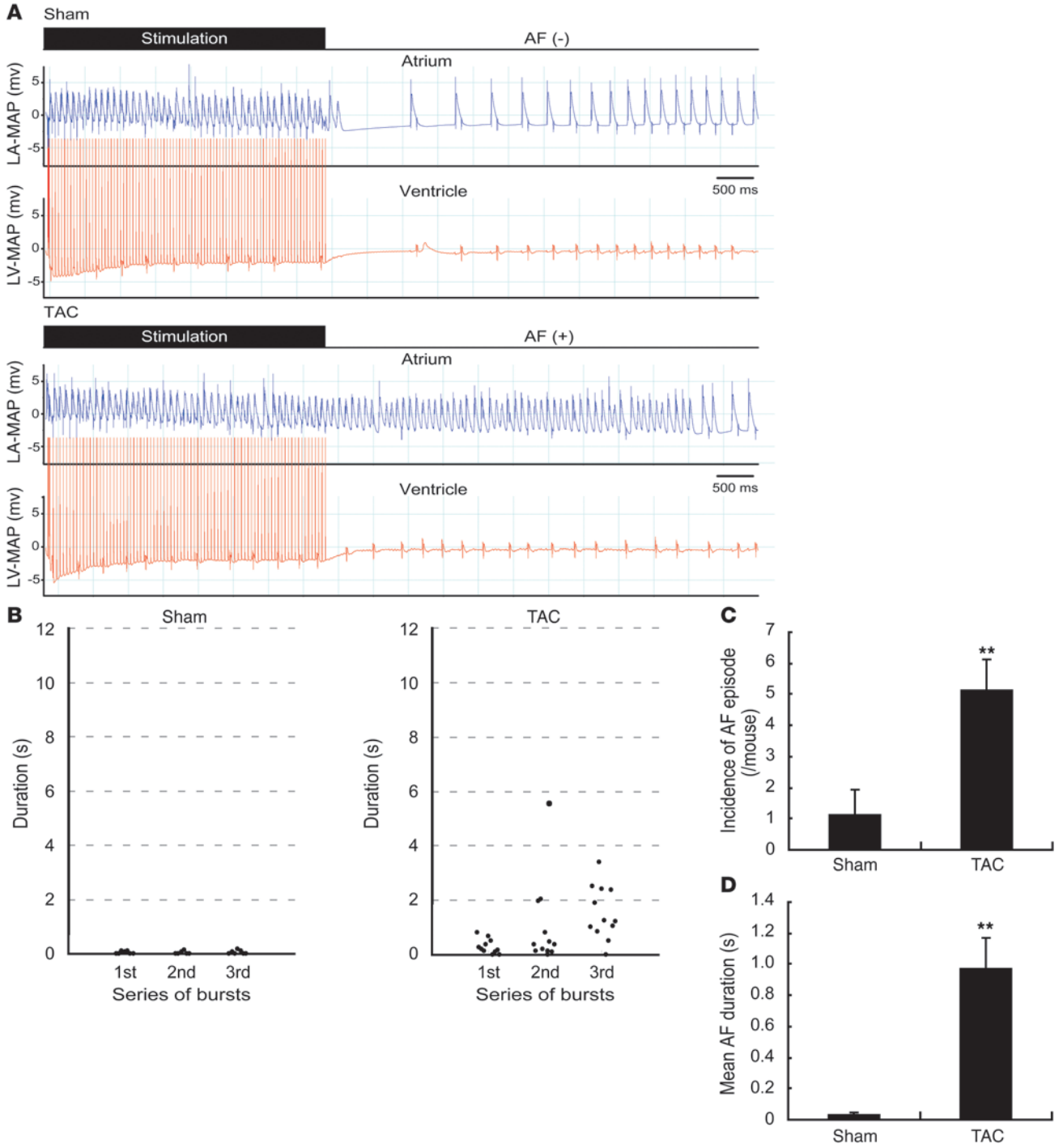

Figure 1

Induction of AF in Langendorff-perfused hearts of mice after TAC operation. (**A**) Termination of the burst of atrial stimulation triggers AF, characterized by rapid and chaotic atrial rhythm and irregular ventricular response, in Langendorff-perfused hearts undergoing TAC operation (lower panels), but not sham operation (upper panels). LA-MAP, monophasic action potential of left atrium; LV-MAP, monophasic action potential of LV. (**B**) AF was triggered in mice undergoing TAC ($n = 5$) or sham ($n = 5$) operation by applying 3 series of bursts with 5-minute intervals. The duration of AF episode occurring after each burst is plotted. (**C**) Incidence of AF episodes during 3 series of bursts in mice undergoing TAC ($n = 5$) or sham ($n = 5$) operation. (**D**) Mean duration of AF episodes during 3 series of bursts in mice undergoing TAC ($n = 5$) or sham ($n = 5$) operation. $^{**}P < 0.01$ versus sham. Data are presented as mean ± SEM.

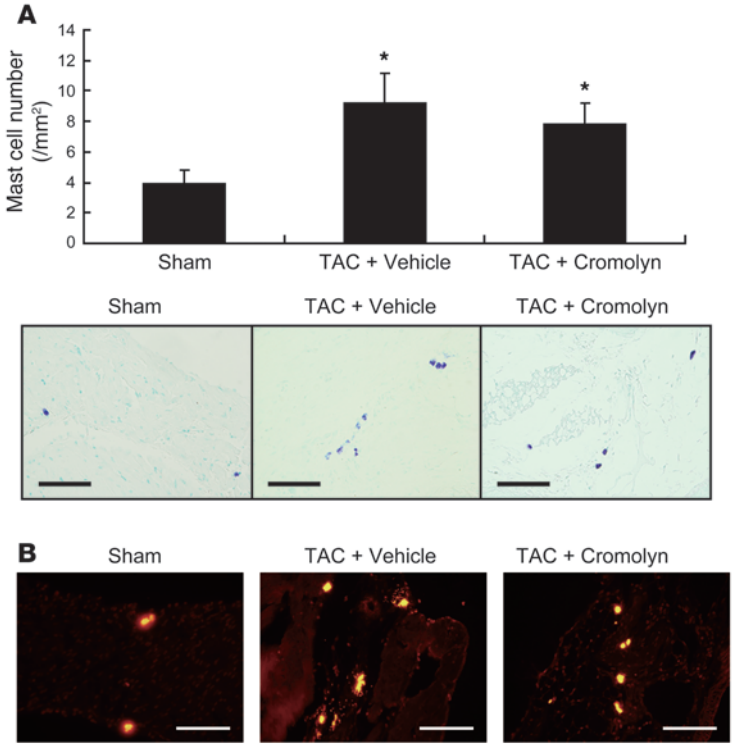

Figure 2
Stabilization of mast cells infiltrating the atrium of TAC-operated mice by cromolyn. (**A**) Representative histological sections with toluidine blue staining for detection of mast cells (purple) in the atrium. Wild-type mice were treated with cromolyn (n = 7) or vehicle (n = 8), and subjected to TAC operation. Mast cell content on day 10 was presented as mean ± SEM. Sham-operated mice were used as control (n = 5). *P < 0.05 versus sham. (**B**) Rhodamine-avidin staining for visualization of mast cell degranulation. Scale bars: 10 μm (**A**); 5 μm (**B**).

idine blue staining, that mast cells were not present in the atrium of mice reconstituted with BM cells from W/W^v mice (W/W^v-BMT mice) after TAC operation, although abundant mast cells infiltrated the atrium of mice reconstituted with BM cells from +/+ mice (+/+-BMT mice) after TAC operation (Figure 4A). Echocardiographic examination revealed that LV hypertrophy after TAC operation did not significantly differ between W/W^v-BMT and +/+-BMT mice, but the fractional shortening in W/W^v-BMT mice was slightly decreased compared with that in +/+-BMT mice (Table 2). In spite of the reduced LV systolic function after TAC operation, the atrium–to–body weight ratios were not significantly different between +/+-BMT mice and W/W^v-BMT mice (0.27 ± 0.02 mg/g vs. 0.31 ± 0.05 mg/g; P = 0.54), and reconstitution with W/W^v BM induced a marked reduction in the incidence and duration of AF episode after atrial burst stimulation compared with +/+ BM reconstitution (Figure 4, B–D). In addition, histological analysis and hydroxyproline assay revealed that atrial fibrosis after TAC operation was attenuated in W/W^v-BMT mice compared with +/+-BMT mice (Figure 4, E and F). These results suggest that deficiency of mast cells prevents atrial structural remodeling and AF inducibility in TAC-operated mice.

BM-derived mast cells cocultured with cardiac myocytes or fibroblasts release PDGF-A to promote fibrinogenesis. In response to a variety of stimuli, mast cells are activated and release numerous bioactive effectors that, either prestored or de novo synthesized, mediate immunoregulatory and proinflammatory effects (11, 24). To delineate mast cell–derived effectors that are involved in the promotion of atrial fibrosis, we examined the gene expressions of fibrosis-related effectors in BM-derived mast cells (BMMCs) after coculture with cardiac myocytes or fibroblasts (Figure 5, A and B, and Supplemental Figure 3). Notably, in quantitative real-time RT-PCR analysis, the mRNA levels of murine *Pdgfa* in BMMCs were prominently elevated after 6 hours coculture with neonatal rat cardiac myocytes or fibroblasts (Figure 5, A and B, and Supplemental Figure 3). In addition, the expression levels of *Pdgfa* were upregulated in the atrium at 10 days after TAC operation, and they were significantly attenuated by reconstitution with W/W^v BM (Figure 5C). These results suggest that mast cells infiltrating the atrium are activated to increase *Pdgfa* gene expression.

Next, we assayed the concentrations of PDGF-AA in medium conditioned by coculture of BMMCs and cardiac fibroblasts. The PDGF-AA concentration showed a more than 3-fold increase after 6 hours coculture, and this increase was remarkably blunted by stabilization of BMMCs with cromolyn during the coculture (Figure 6A). The conditioned medium of coculture promoted cell proliferation of cardiac fibroblasts, and the proliferative effects were abrogated by addition of a neutralizing anti-PDGF α-receptor (anti–PDGFR-α) antibody to the conditioned medium (Figure 6B). Furthermore, the expression of *Col3a1* in cardiac fibroblasts was upregulated after coculture with BMMC, and it was blunted by the treatment with cromolyn or anti–PDGFR-α antibody (Figure 6C). Thus, BMMC-derived PDGF-A can induce cell proliferation and collagen gene expression in cardiac fibroblasts. These results raise a possibility that infiltrating mast cells promote atrial fibrosis and AF inducibility in a PDGF-A–mediated pathway.

Administration of PDGF-AA enhances AF susceptibility in normal hearts. To examine functional significance of atrial *Pdgfa* upregulation in the development of AF substrate, we administered PDGF-AA or vehicle to nonoperated mice and applied atrial burst stimulation. Administration of PDGF-AA for 10 days induced systemic tissue fibrosis, which was particularly prominent in atrium as compared with ventricle (Figure 7A). As a consequence, PDGF-AA–treated hearts showed a significant increase in the incidence and duration of AF episode after atrial burst stimulation under Langendorff perfusion compared with vehicle-treated hearts (Figure 7, B–D). These results suggest that upregulation of *Pdgfa* in atrium can induce atrial fibrosis and enhance AF inducibility in normal hearts.

Neutralization of PDGFR-α attenuates AF in TAC-operated hearts. Next, to examine the role of PDGF-A in the pathogenesis of AF substrate, we inhibited the actions of PDGF-A in TAC-operated hearts by systemic injection of a neutralizing antibody against PDGFR-α (APA5) (27). At 10 days after TAC operation, LV hypertrophy and contraction, as assessed by echocardiography, did not significantly differ between neutralizing antibody–treated mice (TAC-APA5 mice) and control IgG2a-treated mice (TAC-IgG mice) (Table 3). In addition, the atrium–to–body weight ratios were not significantly different between TAC-APA5 and TAC-IgG mice (0.34 ± 0.02 mg/g vs. 0.31 ± 0.03 mg/g; P = 0.44). However, neutralization of PDGFR-α induced a marked reduction

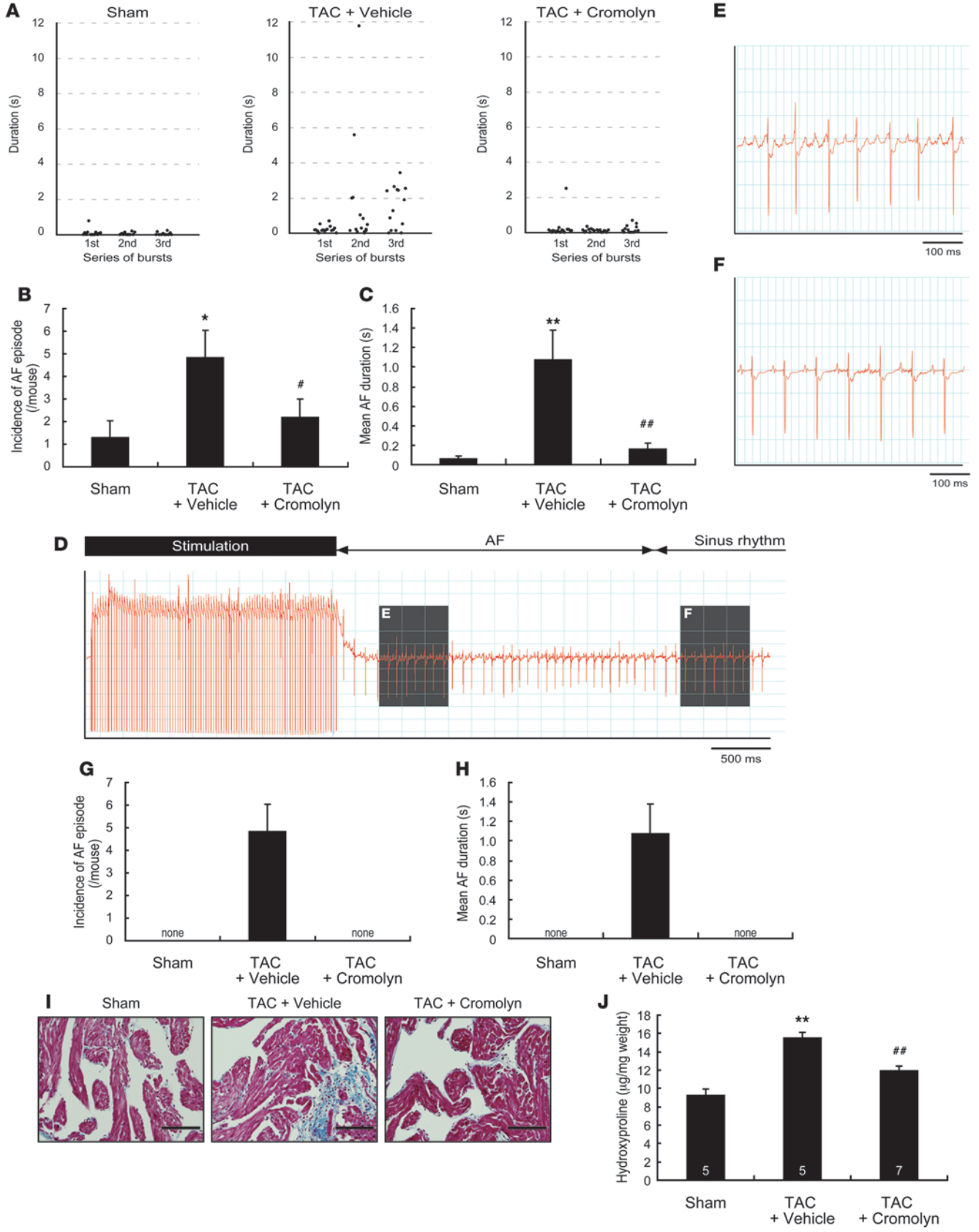
A
Sham
TAC + Vehicle
TAC + Cromolyn
Duration (s)
Series of bursts
1st
2nd
3rd
B
Incidence of AF episode (/mouse)
C
Mean AF duration (s)
Sham
TAC + Vehicle
TAC + Cromolyn
E
F
100 ms
D
Stimulation
AF
Sinus rhythm
500 ms
G
H
none
I
J
Hydroxyproline (μg/mg weight)
5
5
7

Figure 3
Attenuation of AF and atrial fibrosis by mast cell stabilization by cromolyn. (**A**) Scatter plot of the duration of AF episodes occurring during 3 series of bursts in Langendorff-perfused hearts (n = 10). (**B**) Incidence of AF episodes during 3 series of bursts under Langendorff perfusion (n = 10). *P < 0.05 versus sham; #P < 0.05 versus TAC treated with vehicle. (**C**) Mean duration of AF episodes during 3 series of bursts under Langendorff perfusion (n = 10). **P < 0.01 versus sham; ##P < 0.01 versus TAC treated with vehicle. (**D**) Representative surface ECG in lead-II deflection of AF induced by termination of the burst of transesophageal atrial pacing in TAC-operated mice. (**E**) High-magnification view of the section delineated by shaded box in **D**, showing AF with chaotic atrial rhythm and irregular ventricular response. (**F**) High-magnification view of the section delineated by shaded box in **D**. AF was spontaneously converted to sinus rhythm. (**G**) Incidence of AF episodes during 3 series of transesophageal bursts (n = 6). (**H**) Mean duration of AF episodes during 3 series of transesophageal bursts (n = 6). (**I**) Representative histological sections with Masson's trichrome staining for visualization of atrial fibrosis (blue staining). Scale bars: 20 μm. (**J**) Hydroxyproline content in the atrium. Number of mice for each experiment is indicated in the bars. **P < 0.01 versus sham; ##P < 0.01 versus TAC treated with vehicle. Data are presented as mean ± SEM.

in the incidence and duration of AF episode both after atrial burst stimulation under Langendorff perfusion (Figure 8, A–C) and after transesophageal atrial pacing in vivo (Figure 8, D and E). In addition, histological analysis and hydroxyproline assay revealed that atrial fibrosis was attenuated in TAC-APA5 mice compared with TAC-IgG mice (Figure 8, F and G). Thus, the effects of cromolyn treatment or BM reconstitution from W/W^v mice on AF substrate were reproduced by neutralization of PDGFR-α in TAC-operated hearts. These results suggest that PDGF-A mediates the deleterious effects of mast cells to promote atrial fibrosis and AF inducibility.

Discussion

Clinical and experimental studies have suggested that inflammation underlies a susceptible AF substrate, which is characterized by interstitial fibrosis in atrium. Our present study demonstrated a hitherto unknown role of mast cells in the development of a susceptible AF substrate. Mast cells were accumulated and activated in the atrium of pressure-overloaded mice, and pharmacological stabilization or genetic depletion of mast cells prevented atrial structural remodeling and reduced the incidence and duration of AF following atrial burst stimulation. Notably, infiltrating mast cells induced upregulation of PDGF-A in the atrium, and neutral-

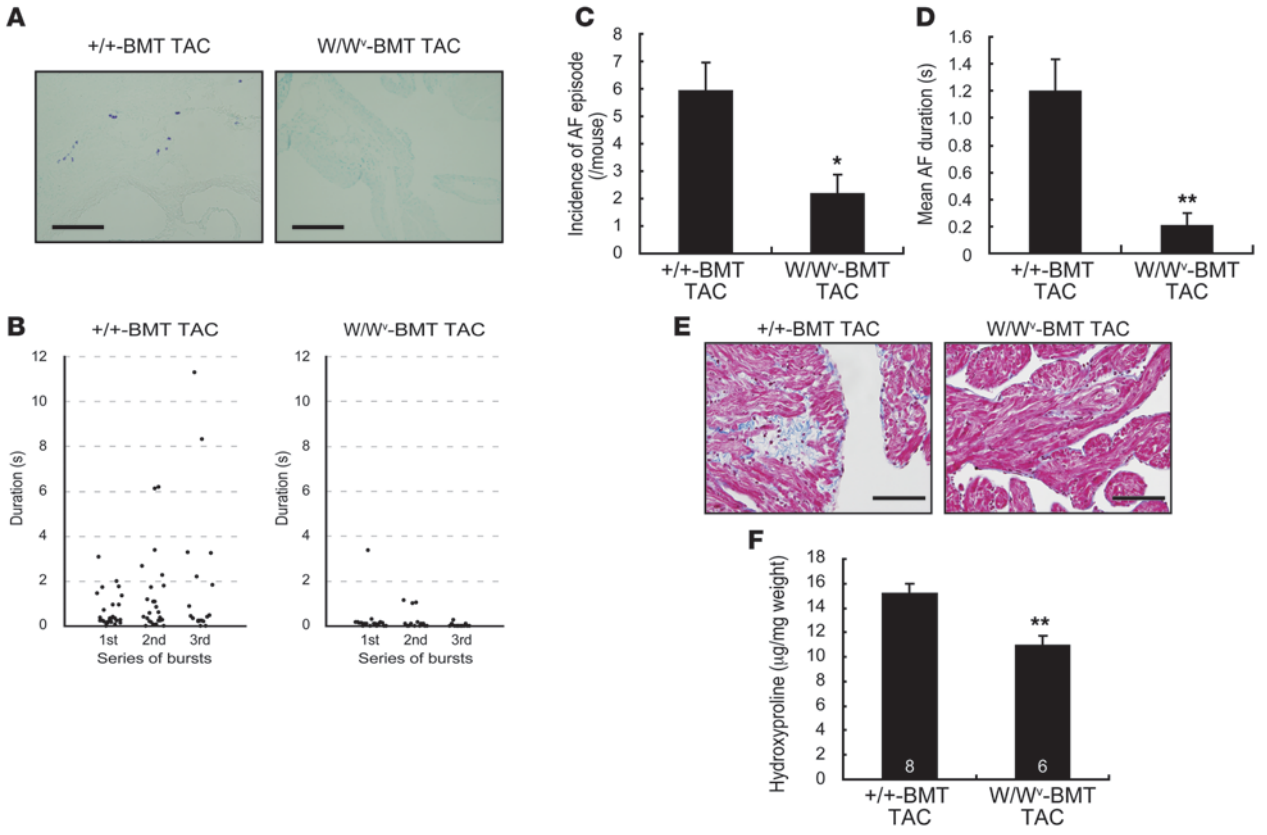

Figure 4
Attenuation of atrial fibrosis and AF by reconstitution with BM cells from W/W^v mice. (**A**) Representative histological sections with toluidine blue staining. Mast cells were not present in the atrium of TAC-operated W/W^v-BMT mice. (**B**) Scatter plot of the duration of AF episodes occurring during 3 series of bursts in TAC-operated W/W^v-BMT mice (n = 11) or +/+-BMT mice (n = 11). (**C**) Incidence of AF episodes during 3 series of bursts (n = 11). *P < 0.05 versus +/+-BMT mice. (**D**) Mean duration of AF episodes during 3 series of bursts (n = 11). **P < 0.01 versus +/+-BMT mice. (**E**) Representative histological sections with Masson's trichrome staining for visualization of atrial fibrosis (blue staining). (**F**) Hydroxyproline content in the atrium. Number of mice for each experiment is indicated in the bars. Scale bars: 10 μm (**A**); 20 μm (**E**). Data are presented as mean ± SEM.

Table 2
Echocardiographic measurements in TAC- or sham-operated W/W^v-BMT or +/+-BMT mice

	Sham		TAC	
	+/+-BMT	W/W^v-BMT	+/+-BMT	W/W^v-BMT
Number	9	9	9	9
HW/BW (mg/g)	4.42 ± 0.14	4.42 ± 0.13	5.51 ± 0.10^A	5.34 ± 0.16^A
HR (bpm)	636.63 ± 7.78	629.22 ± 2.89	613.20 ± 9.34	612.33 ± 6.78
LVDd (mm)	3.68 ± 0.05	3.61 ± 0.07	3.55 ± 0.07	3.69 ± 0.07
LVDs (mm)	2.30 ± 0.05	2.15 ± 0.05	2.05 ± 0.04^A	2.28 ± 0.08^B
FS (%)	39.3 ± 0.93	40.4 ± 0.44	41.6 ± 0.26^C	38.96 ± 1.32^D
LVPWth (mm)	0.61 ± 0.01	0.58 ± 0.01	0.68 ± 0.01^A	0.66 ± 0.02^A

$^A P < 0.01$ versus sham. $^B P < 0.01$ versus TAC-operated +/+-BMT. $^C P < 0.05$ versus sham. $^D P < 0.05$ versus TAC-operated ++-BMT.

ization of PDGFR-α prevented atrial fibrosis and AF inducibility, indicating a pivotal role of PDGF-A in mast cell–triggered AF. It has been reported that atrial arrhythmias and fibrillation occur with extremely low frequency in mice because the atrium is too small in size to maintain multiple-circuit reentry (28). Indeed, we did not detect any spontaneous episode of AF in TAC-operated mice by ECG telemetry (Supplemental Figure 1), but atrial burst stimulation reproducibly induced AF either in ex vivo or in vivo hearts subjected to pressure overload (Figures 1 and 3). Although the duration of AF was limited in length as compared with that in large animal models, a mouse model is powerful for dissection of the causal relationship between arrhythmogenesis and genetic or cellular factors. Although transesophageal pacing in vivo is minimally invasive for atrial stimulation, the incidence of AF was relatively low even in TAC-operated mice (50%), and an anesthetic agent might influence the inducibility and duration of AF in an in vivo model (28). In this regard, atrial stimulation under Langendorff perfusion is a suitable and reliable model of AF that provides mechanistic and therapeutic insights into development of an AF substrate in the setting of hemodynamic overload.

Besides orchestrating allergic and immune responses, mast cells participate in the inflammatory process that underlies the development of cardiovascular diseases (11). Insomuch as the number of infiltrating mast cells at the affected lesions is significantly increased but yet relatively low, it has been difficult to characterize the relevance of these cells to the pathogenesis of a disease. However, mice genetically deficient for mast cells allow assessment of

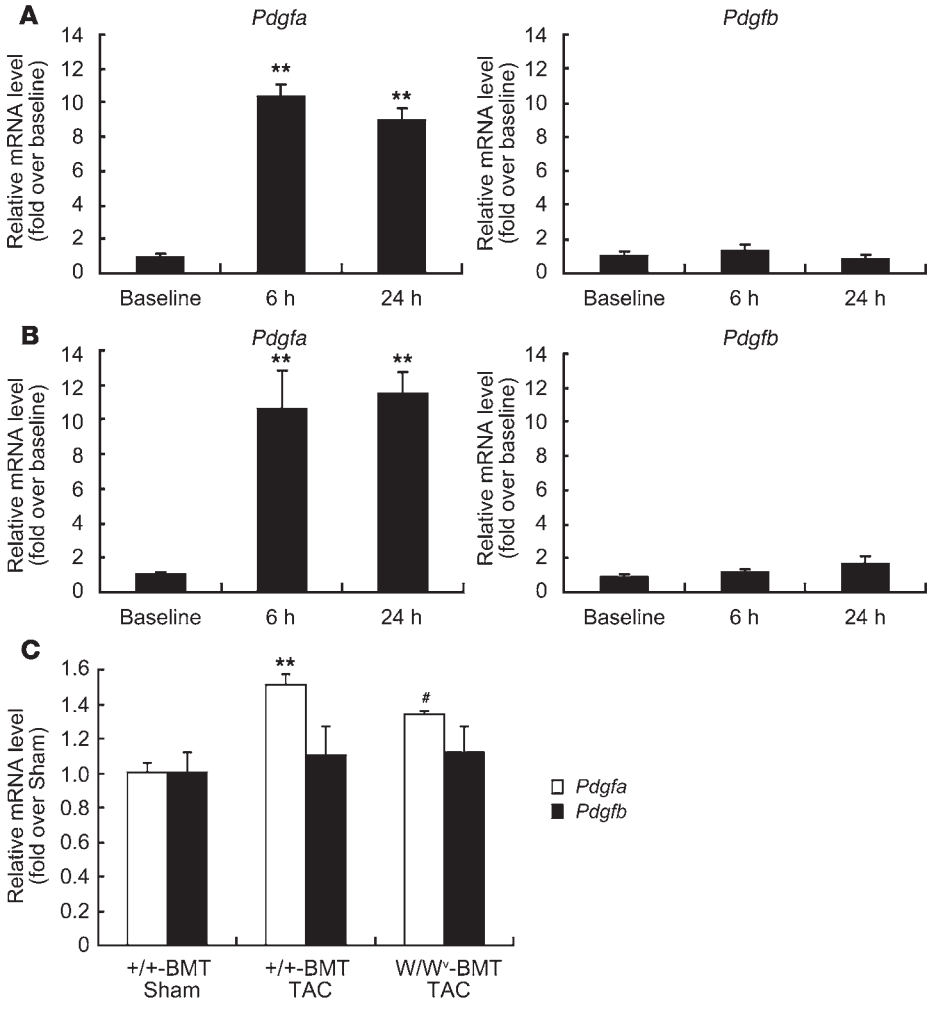

Figure 5
Mast cell–mediated upregulation of *Pdgfa* expression in the atrium of TAC-operated hearts. (**A**) mRNA expression of *Pdgfa* and *Pdgfb* in BMMCs at baseline, 6 hours, and 24 hours after coculture with cardiac myocytes. Experiments were repeated 4 times in triplicate. $^{**}P < 0.01$ versus baseline. (**B**) mRNA expressions of *Pdgfa* and *Pdgfb* in BMMCs at baseline, 6 hours, and 24 hours after coculture with cardiac fibroblasts. Experiments were repeated 5 times in triplicate. $^{**}P < 0.01$ versus baseline. (**C**) mRNA expressions of *Pdgfa* and *Pdgfb* in the atrium of sham-operated mice ($n = 8$), TAC-operated W/W^v-BMT mice (W/W^v-BMT TAC, $n = 7$), or +/+ mice (+/+-BMT TAC, $n = 6$). $^{**}P < 0.01$ versus sham; $^{\#}P < 0.05$ versus +/+-BMT TAC. Data are presented as mean ± SEM.

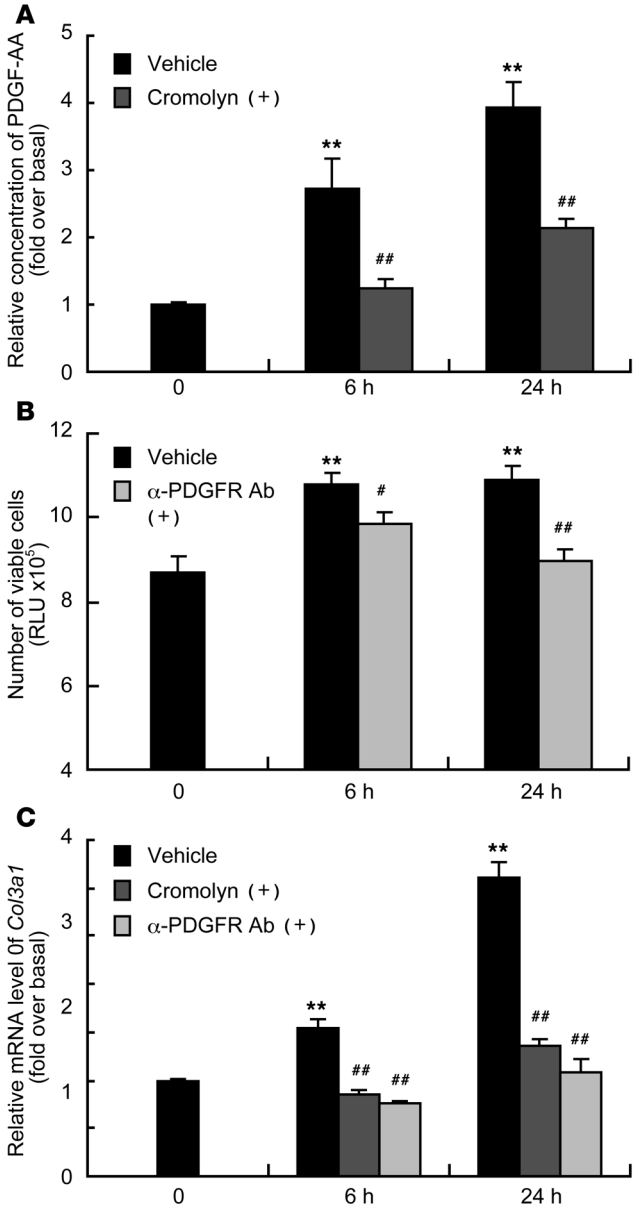

Figure 6
BMMC-derived PDGF-A can induce cell proliferation and collagen gene expression in cardiac fibroblasts. (**A**) ELISA analysis of PDGF-AA content in conditioned medium at baseline, 6 hours, and 24 hours after coculture of BMMCs and cardiac fibroblasts with or without cromolyn (10 μM). Experiments were repeated 5 times in triplicate. $^{**}P < 0.01$ versus baseline; $^{\#\#}P < 0.01$ versus vehicle. (**B**) Number of viable cardiac fibroblasts at baseline, 6 hours, and 24 hours after culture in medium-conditioned coculture of BMMCs and cardiac fibroblasts with or without a neutralizing anti–PDGFR-α antibody (2 μg/ml), as assessed by relative amount of ATP. Experiments were repeated 4 times in triplicate. $^{**}P < 0.01$ versus baseline; $^{\#}P < 0.05$; $^{\#\#}P < 0.01$ versus vehicle. (**C**) mRNA expressions of *Col3a1* in cardiac fibroblasts cocultured with BMMCs with or without cromolyn (10 μM) or a neutralizing anti–PDGFR-α antibody (2 μg/ml) at baseline, 6 hours, and 24 hours. Experiments were repeated 4 times in triplicate. $^{**}P < 0.01$ versus baseline; $^{\#\#}P < 0.01$ versus vehicle. Data are presented as mean ± SEM.

the contributions of mast cell function to biological responses in vivo (11). In this study, we utilized *c-kit* mutant W/W^v mice that are profoundly mast cell deficient (29) and virtually lack melanocytes and interstitial Cajal cells (30). According to a recent paper, *c-kit* is also expressed in cardiac stem cells and cardiac myocytes and plays a regulatory role in the differentiation of these cells (31). Thus, to avoid the effects of *c-kit* mutation on cardiac myocytes, we reconstituted C57BL/6 mice with BM from W/W^v mice. BM reconstitution from W/W^v mice influenced contractile function, which might be related to hematological abnormalities such as macrocytic anemia (32). In spite of the hemodynamic burden, atrial structural remodeling and AF susceptibility were blunted by BM reconstitution from W/W^v mice, which underpinned the functional importance of mast cells in the AF pathogenesis of pressure-overloaded hearts.

Mast cells exist in the heart under physiological conditions (13), and mast cell density in heart tissues of patients with cardiomyopathy is elevated, as compared with normal hearts (33). Mast cells are long lived in the tissue and can reenter cell cycle and proliferate locally (34). A variety of chemokines have been identified that induce local recruitment of mast cells, such as SCF, monocyte chemoattraction protein-1 (MCP-1), nerve growth factor (NGF), and RANTES (24). In addition, interactions between mast cells and connective tissue matrix components have profound influences on the distribution of mast cells in tissues (35–37). Although the most important trigger for mast cell activation is antigen- and IgE-dependent aggregation of IgE receptor (FcεRI), mast cells can be activated by various factors, such as cytokines, growth factors, and hormones (11, 12, 24). In our study, coculture with cardiac myocytes or fibroblasts per se promoted gene expression of some cytokines in BMMCs. We postulate that a certain paracrine- or cell-to-cell contact–dependent signaling may trigger mast cell activation in hearts. Further investigation will be required to delineate the precise mechanisms of how cardiac mast cells are accumulated and activated in stressed hearts.

Mast cells secrete diverse chemical mediators, cytokines, and growth factors upon exposure to a stimulus. This process involves release of the mediators prestored in the granules (degranulation) and de novo synthesis of mediators. Differential synthesis of mast cell mediators is dependent on the particular mechanism of activation and the strength of the stimulus and is crucially involved in the inflammatory process (12, 24). We identified PDGF-A as a crucial molecule that mediates mast cell–induced atrial fibrosis. Among the fibrogenic mediators, upregulation of *Pdgfa* in BMMCs was pronounced after coculture either with cardiac myocytes or fibroblasts. In our coculture experiments, BMMC-derived PDGF-A accelerated proliferation of cardiac fibroblasts and stimulated synthesis of type III collagen in cardiac fibroblasts. PDGF-A dimeric isoform (PDGF-AA) selectively binds to PDGFR-α (38), and PDGF-AA infusion exerted potent fibrogenic effects, particularly on atrium (Figure 7A), consistent with a previous paper demonstrating that atrial fibroblasts showed higher reactivity to PDGF than ventricular fibroblasts (39). Importantly, the mRNA levels of *Pdgfa* in atrium were significantly increased after TAC operation, which was blunted by depletion of mast cells by BM reconstitution from W/W^v mice. PDGF-A production in atrium is critically relevant to the AF pathogenesis of pressure-overloaded hearts because neutralization of PDGFR-α prevented atrial fibrosis and AF. Collectively, our results suggest that atrial mast cells induce upregulation

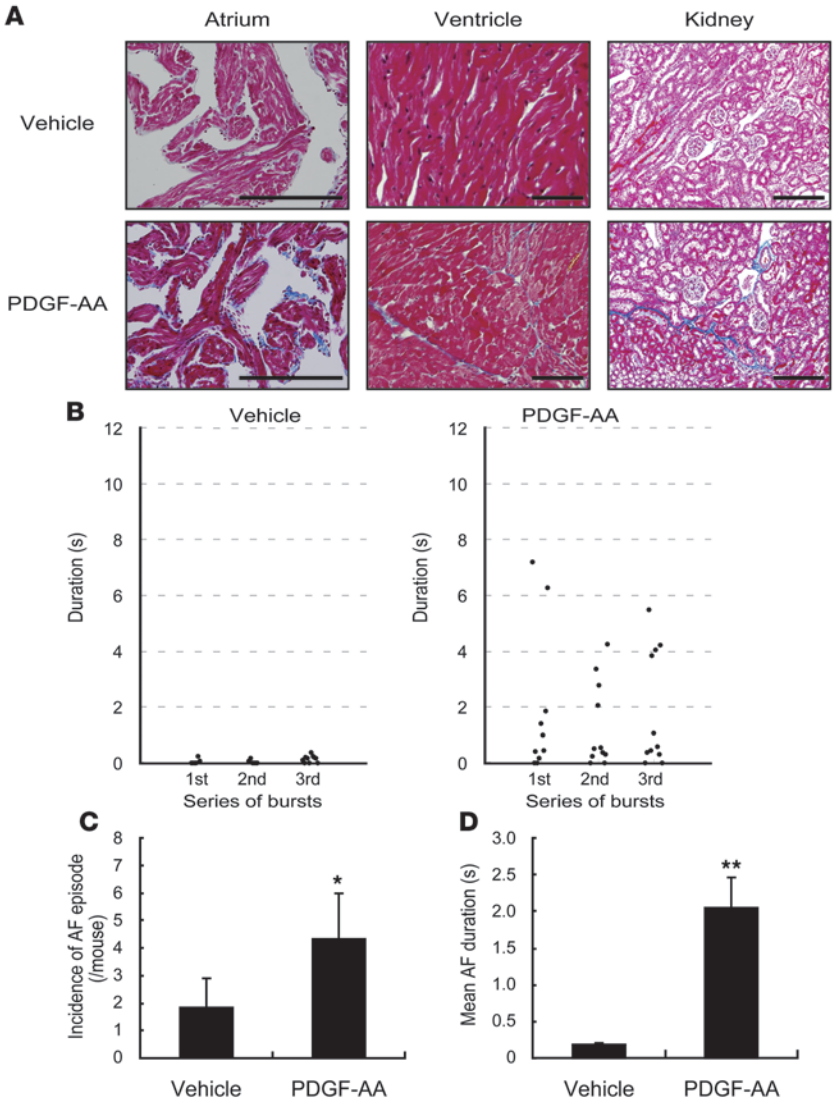

Figure 7
Systemic administration of PDGF-AA induces atrial fibrosis and enhances AF susceptibility in Langendorff-perfused hearts. (**A**) Representative histological sections with Masson's trichrome staining for visualization of fibrosis (blue staining) in the atrium, ventricle, and kidney of mice administered PDGF-AA or vehicle. Scale bars: 20 μm. (**B**) Scatter plot of the duration of AF episodes occurring during 3 series of bursts in mice administered PDGF-AA ($n = 6$) or vehicle ($n = 6$). Duration of AF episodes occurring after each burst are plotted. (**C**) Incidence of AF episodes during 3 series of bursts in mice administered PDGF-AA ($n = 6$) or vehicle ($n = 6$). (**D**) Mean duration of AF episodes during 3 series of bursts in mice administered PDGF-AA ($n = 6$) or vehicle ($n = 6$). Data are presented as mean ± SEM. $^{*}P < 0.05$ versus vehicle; $^{**}P < 0.01$ versus vehicle.

of *Pdgfa*, leading to progression of a susceptible AF substrate in pressure-overloaded hearts. At present, it remains uncertain whether atrial mast cells are the sole source of PDGF-A. Indeed, mast cell activation can influence the function of many different cell types (12, 24), and especially, macrophages may serve as a source of PDGF-A (38). Further studies using an intricate genetic model to delete *Pdgfa* specifically in mast cells will be required to dissect the importance of mast cell–derived PDGF-A in the pathogenesis of AF.

Several clinical studies have proved the efficacy of pharmacological inhibition of the renin-angiotensin system in the prevention of atrial fibrosis and promotion of AF (40). The therapeutic approach to attenuating or reversing the AF substrate is appealing. Our study highlighted the pathogenic role of mast cells in promoting the AF substrate in pressure-overloaded hearts. Of course, this observation must be further investigated in future studies using large animal models for testing applicability to clinical conditions because variability among species and experimental models may give rise to differences in anatomical and electrophysiological parameters (41). As a starting point for investigations, we propose that the mast cell–PDGF-A axis will be a promising therapeutic target for the upstream prevention of AF in stressed hearts.

Methods

Mice, TAC operation, and echocardiography. All of the experimental protocols were approved by the Institutional Animal Care and Use Committee of Chiba University. C57BL/6 mice, mast cell–deficient W/W^{v} mice, and congenic +/+ littermates were purchased from Japan SLC. For TAC operation, 10-week-old male mice were anesthetized by i.p. injection of pentobarbital, and respiration was artificially controlled with a tidal volume of 0.2 ml and a respiratory rate of 110 breaths/min. The transverse aorta was constricted with 7-0 nylon strings by ligating the aorta with splinting a blunted 27-gauge needle, which was removed after the ligation. After aortic constriction, the chest was closed and mice were allowed to recover from anesthesia. We confirmed that the magnitude of initial pressure elevation after aortic banding was identical in all groups of mice. The surgeon had no information about the mice used in this study. For evaluation of cardiac dimensions and contractility, transthoracic echocardiography was performed on conscious mice with the Vevo 770 Imaging System using a 25-MHz linear probe (Visual Sonics).

Table 3
Echocardiographic measurements in TAC-APA5 or TAC-IgG mice

	TAC-IgG	TAC-APA5
Number	10	10
HW/BW (mg/g)	5.71 ± 0.18	5.67 ± 0.16
HR (bpm)	633.30 ± 16.06	657.00 ± 11.91
LVDd (mm)	3.54 ± 0.09	3.59 ± 0.08
LVDs (mm)	2.07 ± 0.09	2.01 ± 0.09
FS (%)	41.7 ± 1.48	44.2 ± 1.51
LVPWth (mm)	0.84 ± 0.01	0.81 ± 0.01

Mast cell stabilization and BM reconstitution. For stabilization of mast cells, cromolyn (50 mg/kg/day; Sigma-Aldrich) or vehicle was administrated daily to mice by i.p. injection (14) for the duration of the experiment (10 days after TAC operation). For BM reconstitution, BM cell suspensions were harvested by flushing the femurs and tibias of 8-week-old W/W^v or +/+ mice. The 5-week-old C57BL/6 mice were preconditioned with total body irradiation (9.5 Gy) 6 hours before transplantation. BM cell suspensions (1.0×10^7 cells per mouse) were transfused via the tail vein to the preconditioned recipient mice. The recipient mice were subjected to BM reconstitution for 6 weeks and were subjected to TAC operation.

Induction of AF in ex vivo and in vivo hearts. For induction of AF in ex vivo hearts, hearts were rapidly excised after i.p. injection of heparin (0.5 U/g) and urethane (2 mg/g) and immediately mounted onto a Langendorff perfusion apparatus (42). The hearts were perfused with a nonrecirculating Krebs-Henseleit buffer (119 mM NaCl, 4.8 mM KCl, 1.2 mM KH_2PO_4, 1.2 mM $MgSO_4$, 2.5 mM $CaCl_2$, 10 mM glucose, and 24.9 mM $NaHCO_3$), which was equilibrated with 5% CO_2/95% O_2 at 37°C. All isolated hearts were stabilized for 5 minutes by perfusion at constant flow (3.0 ± 0.2 ml/min) before programmed electrical stimulation. The whole system temperature was kept at 37°C. Two chlorinated silver wires were placed on the base of the heart as indifferent and common ground electrodes. A pair of recording electrodes were placed on the apex and anterior wall of the heart to record ventricular electrograms. Bipolar stimulating electrodes were pressed against the right atrium surface, and bipolar recording electrodes were placed on the left atrium surface to record atrial electrograms.

For induction of AF in in vivo hearts, mice were anesthetized with i.p. injection of pentobarbital and supported by artificial ventilation. The body temperature of mice was monitored and kept at 37°C using a heating pad during the experiments. A 2-French catheter electrode (Japan Lifeline) was placed at the esophageal position dorsal to the left atrium. A surface ECG was simultaneously recorded using electrodes in a lead-II configuration.

Inducibility of AF was tested by applying a 2-second burst using the automated stimulator. The first 2-second burst had a cycle length (CL) of 40 ms, decreasing in each successive burst with a 2-microsecond decrement down to a CL of 20 ms. A series of bursts was repeated 3 times after stabilization for 5 minutes. AF duration was defined as the interval between the rapid irregular atrial rhythm triggered after the bursts and the onset of first normal sinus beat.

Histological analysis. Hearts were excised and immediately fixed in 10% neutralized formalin, and they were then embedded in paraffin. Serial sections of atrium at 5 μm were stained with Masson's trichrome for evaluation of fibrosis. We determined mast cell number and morphology with toluidine blue staining (0.1%; Sigma-Aldrich) and rhodamine-avidin staining (1:100; Vector Laboratories) (20, 26). Specificity of mast cell detection was confirmed by staining sections of W/W^v and +/+ mice at the same dilution of the reagent. The total number of mast cells was counted manually and blindly in 3 microscopic sections from each mouse, and the total area was determined using computer-assisted image analysis (ImageJ; http://rsbweb.nih.gov/ij/).

Hydroxyproline assay. We evaluated collagen content in the atrium by quantification of hydroxyproline, as described previously (43). In brief, the atrium was weighed and then hydrolyzed in 6 N HCl at 100°C overnight. Hydrolyzed tissue was neutralized with NaOH, vacuum dried at 50°C, and resuspended in 1 ml of 5 mM HCl. An aliquot of 20 μl hydrolyzed tissue was added to 180 μl of H_2O in a glass tube. Thereafter, we mixed 100 μl of chloramine-T solution (0.14 g chloramine-T, Sigma-Aldrich; 2 ml H_2O, 8 ml hydroxyproline assay buffer) with the diluted hydrolyzed tissue solution. The ingredients of hydroxyproline assay buffer were as follows: 11.4 g sodium acetate anhydrous (Sigma-Aldrich), 7.5 g trisodium citrate dihydrate (Sigma-Aldrich), 40 ml H_2O (pH adjusted to 6.0), and 77 ml isopropanol, bringing the final volume to 200 ml with H_2O. After incubation for 10 minutes at room temperature, 1.25 ml Ehrlich's reagent (6.0 g p-dimethylaminobenzaldehyde [Sigma-Aldrich], 18 ml 60% perchlorate [Fluka], 78 ml isopropanol) was added and mixed. The samples were incubated at 55°C for 20–25 minutes, and the sample absorbance was read at 558 nm. We used *trans*-4-hydroxy-L-proline (Sigma-Aldrich) (ranging from 0 to 4 mg) to draw the standard curve.

Coculture of BMMCs with cardiac myocytes or fibroblasts. The BM cells were harvested from C57BL/6 mice and cultured for 5 weeks in RPMI 1640 medium (GIBCO; Invitrogen) supplemented with 10% FBS (Equitech-Bio), 0.1 mM MEM Non-Essential Amino Acids Solution (GIBCO; Invitrogen), 4 mM L-glutamine, 25 mM HEPES, 1 mM sodium pyruvate, 50 μM β-mercaptoethanol, 100 U/ml penicillin, 100 μg/ml streptomycin, and 30 ng/ml of recombinant murine IL-3 (PeproTech GmbH) at 37°C in 5% CO_2 (44). By 5 weeks in culture, mast cells were enriched to more than 95%, as assessed by the presence of metachromatic granules in toluidine blue–stained cells and by cell-surface expression of FcεRI (Upstate) using flow cytometric analysis. The cardiac myocytes and fibroblasts were prepared from hearts of 1-day-old Wistar rats, as described previously (45). Dissociated cells were preplated onto 10-cm culture dishes for 30 minutes, which permitted preferential attachment of fibroblasts to the bottom of the dish. Nonadherent cardiac myocytes (3.5×10^5 cells/3.5-cm dish) or adherent fibroblasts (2.0×10^6 cells/3.5-cm dish) were plated on 3.5-cm dishes and cultured for 24 hours in medium (DMEM [GIBCO; Invitrogen], supplemented with 10% FBS, 100 U/ml penicillin, and 100 μg/ml streptomycin). The cells were starved under a serum-free condition for 24 hours before initiation of the coculture. BMMCs (5.0×10^6 cells/3.5-cm dish) were placed onto layers of cardiac myocytes or fibroblasts and were continuously cocultured in DMEM without supplementation with FBS. For stabilization of BMMCs in vitro, BMMCs were pretreated with 10^{-5} M cromolyn (Sigma-Aldrich) for 30 minutes before initiation of coculture, and cromolyn treatment was continued throughout the coculture.

Real-time RT-PCR analysis. Total RNA was extracted by using RNeasy Kit (QIAGEN), and single-stranded cDNA was transcribed by using QuantiTect Reverse Transcription Kit (QIAGEN) according to the manufacturer's protocol. We conducted quantitative real-time PCR analysis with the Universal ProbeLibrary Assays (Roche Applied Science) according to the manufacturer's instructions. Amplification conditions were as follows: initial denaturation for 10 minutes at 95°C followed by 45 cycles of 10 seconds at 95°C and 25 seconds at 60°C. Individual PCR products were analyzed by melting-point analysis. The expression level of a gene was normalized relative to that of *Gapdh* by using a comparative Ct method. The primer sequences and universal probe numbers were designed with the ProbeFinder software as follows: *Pdgfa*, 5′-GTGCGACCTCCAACCTGA-3′ and 5′-GGCTCATCT-CACCTCACATCT-3′, no. 52; *Pdgfb*, 5′-CGGCCTGTGACTAGAAGTCC-3′ and 5′-GAGCTTGAGGCGTCTTGG-3′, no. 32; *Col3a1*, 5′-TCCCCTG-

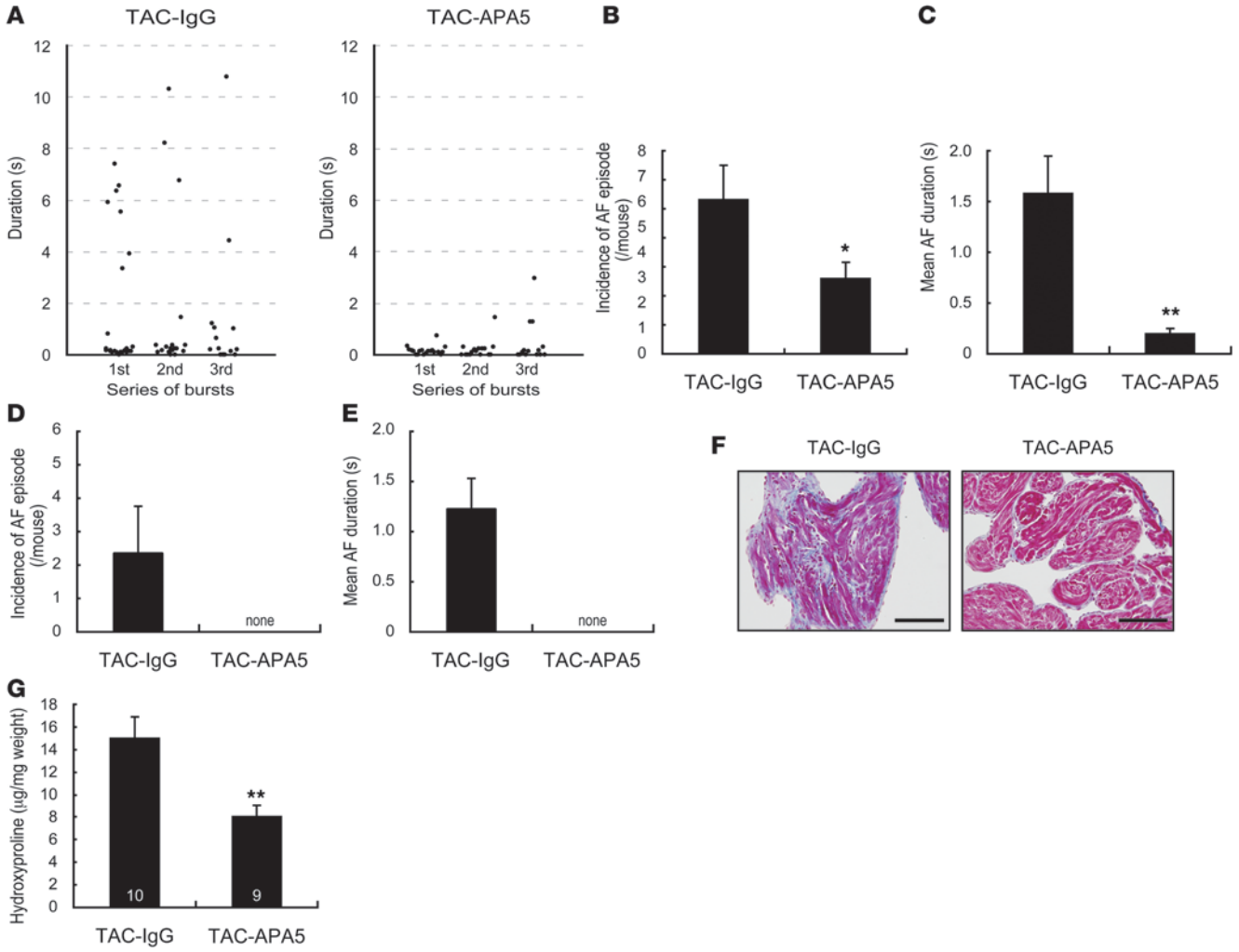

Figure 8

Attenuation of atrial fibrosis and AF by neutralization of PDGFR-α. (**A**) Scatter plot of duration of AF episodes occurring during 3 series of bursts under Langendorff perfusion in TAC-APA5 ($n = 9$) or TAC-IgG mice ($n = 9$). (**B**) Incidence of AF episodes during 3 series of bursts under Langendorff perfusion ($n = 9$). *$P < 0.05$ versus control IgG. (**C**) Mean duration of AF episodes during 3 series of bursts under Langendorff perfusion ($n = 9$). **$P < 0.01$ versus control IgG. (**D**) Incidence of AF episodes during 3 series of transesophageal bursts ($n = 6$). (**E**) Mean duration of AF episodes during 3 series of transesophageal bursts ($n = 6$). (**F**) Representative histological sections with Masson's trichrome staining for visualization of atrial fibrosis (blue staining). Scale bars: 20 μm. (**G**) Hydroxyproline content in the atrium ($n = 9$). Number of mice for each experiment is indicated in the bars. **$P < 0.01$ versus control IgG. Data are presented as mean ± SEM.

GAATCTGTGAATC-3′ and 5′-TGAGTCGAATTGGGGAGAAT-3′, no. 49; mouse *Gapdh*, 5′-TGTCCGTCGTGGATCTGAC-3′ and 5′-CCTGCTTCACCACCTTCTTG-3′, no. 80; rat *Gapdh*, 5′-TGGGAAGCTGGTCATCAAC-3′ and 5′-GCATCACCCCATTTGATGTT-3′, no. 9.

ELISA of PDGF-AA. The concentrations of PDGF-AA in the conditioned medium were assayed by using Human/Mouse PDGF-AA Quantikine ELISA Kit (R&D Systems) according to the manufacturer's protocol.

Cell proliferation assay. Cardiac fibroblasts (2×10^4 cells/well) were plated on a 48-well plate and were cultured for 24 hours in medium (DMEM supplemented with 10% FBS, 100 U/ml penicillin, and 100 μg/ml streptomycin) at 37°C in 5% CO_2. After 24 hours of starvation under serum-free conditions, we replaced the medium with that conditioned by coculture of BMMCs and cardiac fibroblasts. After 24 hours of culture, cells were harvested, and subjected to semiquantification of the viable cell numbers that are proportional to the amount of ATP by using CellTiter-Glo Luminescent Cell Viability Assay Kit (Promega).

Systemic administration of PDGF-AA. Mini-osmotic pumps (model 2002; Alzet) were subcutaneously implanted in 10-week-old male mice to deliver recombinant murine PDGF-AA (0.2 μg/day; PeproTech) or vehicle. At 10 days after implantation, mice were sacrificed for analysis.

Inhibition of PDGF-A by a neutralizing anti–PDGFR-α antibody. To antagonize the effects of BMMC-derived PDGF-A in vitro, we pretreated BMMCs with 2 μg/ml of clone APA5 (200 μg/day) (27) or control IgG2a (eBioscience) for 30 minutes before initiation of coculture and continued the treatment throughout the coculture. To inhibit the effects of PDGF-A in vivo, we administered anti–PDGFR-α antibody (200 μg/day) (27) or control IgG2a by i.p. injection to mice for the duration of the experiment (10 days after TAC operation). APA5, a rat monoclonal anti–mouse PDGFR-α antibody (IgG2a), was described previously (46).

Statistics. All data are presented as means ± SEM. Two-group comparison was analyzed by unpaired 2-tailed Student's *t* test, and multiple-group comparison was performed by 1-way ANOVA followed by the Fisher's pro-

tected least significant difference test for comparison of means. $P < 0.05$ was considered to be statistically significant.

Acknowledgments

We are grateful to S. Nishikawa (Center for Developmental Biology, RIKEN, Japan) for providing APA5 hybridoma cells. We thank A. Furuyama, M. Ikeda, Y. Ohtsuki, I. Sakamoto, and M. Kikuchi for their excellent technical assistance. This work was supported in part by grants from the Japanese Ministry of Education, Science, Sports, and Culture, and Health and Labor Sciences Research grants (to I. Komuro and H. Akazawa); and grants from Japan Intractable Diseases Research Foundation and Takeda Science Foundation (to H. Akazawa).

Received for publication May 21, 2009, and accepted in revised form October 14, 2009.

Address correspondence to: Issei Komuro, Department of Cardiovascular Science and Medicine, Chiba University Graduate School of Medicine, 1-8-1 Inohana, Chuo-ku, Chiba 260-8670, Japan. Phone: 81-43-226-2097; Fax: 81-43-226-2557; E-mail: komuro-tky@umin.ac.jp.

1. Fuster V, et al. ACC/AHA/ESC 2006 guidelines for the management of patients with atrial fibrillation. *Circulation*. 2006;114(7):e257–354.
2. Nattel S. New ideas about atrial fibrillation 50 years on. *Nature*. 2002;415(6868):219–226.
3. Burstein B, Nattel S. Atrial fibrosis: mechanisms and clinical relevance in atrial fibrillation. *J Am Coll Cardiol*. 2008;51(8):802–809.
4. Corradi D, Callegari S, Maestri R, Benussi S, Alfieri O. Structural remodeling in atrial fibrillation. *Nat Clin Pract Cardiovasc Med*. 2008;5(12):782–796.
5. Frustaci A, et al. Histological substrate of atrial biopsies in patients with lone atrial fibrillation. *Circulation*. 1997;96(4):1180–1184.
6. Issac TT, Dokainish H, Lakkis NM. Role of inflammation in initiation and perpetuation of atrial fibrillation: a systematic review of the published data. *J Am Coll Cardiol*. 2007;50(21):2021–2028.
7. Nakamura Y, et al. Tissue factor expression in atrial endothelia associated with nonvalvular atrial fibrillation: possible involvement in intracardiac thrombogenesis. *Thromb Res*. 2003;111(3):137–142.
8. Verheule S, et al. Alterations in atrial electrophysiology and tissue structure in a canine model of chronic atrial dilatation due to mitral regurgitation. *Circulation*. 2003;107(20):2615–2622.
9. Chung MK, et al. C-reactive protein elevation in patients with atrial arrhythmias: inflammatory mechanisms and persistence of atrial fibrillation. *Circulation*. 2001;104(24):2886–2891.
10. Aviles RJ, et al. Inflammation as a risk factor for atrial fibrillation. *Circulation*. 2003;108(24):3006–3010.
11. Kalesnikoff J, Galli SJ. New developments in mast cell biology. *Nat Immunol*. 2008;9(11):1215–1223.
12. Metz M, Grimbaldeston MA, Nakae S, Piliponsky AM, Tsai M, Galli SJ. Mast cells in the promotion and limitation of chronic inflammation. *Immunol Rev*. 2007;217:304–328.
13. Sperr WR, et al. The human cardiac mast cell: localization, isolation, phenotype, and functional characterization. *Blood*. 1994;84(11):3876–3884.
14. Bot I, et al. Perivascular mast cells promote atherogenesis and induce plaque destabilization in apolipoprotein E-deficient mice. *Circulation*. 2007;115(19):2516–2525.
15. Sun J, et al. Mast cells promote atherosclerosis by releasing proinflammatory cytokines. *Nat Med*. 2007;13(6):719–724.
16. Sun J, et al. Mast cells modulate the pathogenesis of elastase-induced abdominal aortic aneurysms in mice. *J Clin Invest*. 2007;117(11):3359–3368.
17. Tsuruda T, et al. Adventitial mast cells contribute to pathogenesis in the progression of abdominal aortic aneurysm. *Circ Res*. 2008;102(11):1368–1377.
18. Hara M, et al. Evidence for a role of mast cells in the evolution to congestive heart failure. *J Exp Med*. 2002;195(3):375–381.
19. Higuchi H, et al. Mast cells play a critical role in the pathogenesis of viral myocarditis. *Circulation*. 2008;118(4):363–372.
20. Mackins CJ, et al. Cardiac mast cell-derived renin promotes local angiotensin formation, norepinephrine release, and arrhythmias in ischemia/reperfusion. *J Clin Invest*. 2006;116(4):1063–1070.
21. Cairns JA, Walls AF. Mast cell tryptase stimulates the synthesis of type I collagen in human lung fibroblasts. *J Clin Invest*. 1997;99(6):1313–1321.
22. Kondo S, et al. Role of mast cell tryptase in renal interstitial fibrosis. *J Am Soc Nephrol*. 2001;12(8):1668–1676.
23. Mori R, Shaw TJ, Martin P. Molecular mechanisms linking wound inflammation and fibrosis: knockdown of osteopontin leads to rapid repair and reduced scarring. *J Exp Med*. 2008;205(1):43–51.
24. Theoharides TC, Kempuraj D, Tagen M, Conti P, Kalogeromitros D. Differential release of mast cell mediators and the pathogenesis of inflammation. *Immunol Rev*. 2007;217:65–78.
25. Sano M, et al. p53-induced inhibition of Hif-1 causes cardiac dysfunction during pressure overload. *Nature*. 2007;446(7134):444–448.
26. Tharp MD, Seelig LL Jr, Tigelaar RE, Bergstresser PR. Conjugated avidin binds to mast cell granules. *J Histochem Cytochem*. 1985;33(1):27–32.
27. Zymek P, et al. The role of platelet-derived growth factor signaling in healing myocardial infarcts. *J Am Coll Cardiol*. 2006;48(11):2315–2323.
28. Olgin JE, Verheule S. Transgenic and knockout mouse models of atrial arrhythmias. *Cardiovasc Res*. 2002;54(2):280–286.
29. Kitamura Y, Go S, Hatanaka K. Decrease of mast cells in W/Wv mice and their increase by bone marrow transplantation. *Blood*. 1978;52(2):447–452.
30. Huizinga JD, et al. W/kit gene required for interstitial cells of Cajal and for intestinal pacemaker activity. *Nature*. 1995;373(6512):347–349.
31. Li M, et al. c-kit is required for cardiomyocyte terminal differentiation. *Circ Res*. 2008;102(6):677–685.
32. Lewis JP, O'Grady LF, Bernstein SE, Russell EE, Trobaugh FE, Jr. Growth and differentiation of transplanted W/Wv marrow. *Blood*. 1967;30(5):601–616.
33. Patella V, et al. Stem cell factor in mast cells and increased mast cell density in idiopathic and ischemic cardiomyopathy. *Circulation*. 1998;97(10):971–978.
34. Galli SJ, et al. Mast cells as "tunable" effector and immunoregulatory cells: recent advances. *Annu Rev Immunol*. 2005;23:749–786.
35. Thompson HL, Burbelo PD, Segui-Real B, Yamada Y, Metcalfe DD. Laminin promotes mast cell attachment. *J Immunol*. 1989;143(7):2323–2327.
36. Dastych J, Costa JJ, Thompson HL, Metcalfe DD. Mast cell adhesion to fibronectin. *Immunology*. 1991;73(4):478–484.
37. Bianchine PJ, Burd PR, Metcalfe DD. IL-3-dependent mast cells attach to plate-bound vitronectin. Demonstration of augmented proliferation in response to signals transduced via cell surface vitronectin receptors. *J Immunol*. 1992;149(11):3665–3671.
38. Bonner JC. Regulation of PDGF and its receptors in fibrotic diseases. *Cytokine Growth Factor Rev*. 2004;15(4):255–273.
39. Burstein B, Libby E, Calderone A, Nattel S. Differential behaviors of atrial versus ventricular fibroblasts: a potential role for platelet-derived growth factor in atrial-ventricular remodeling differences. *Circulation*. 2008;117(13):1630–1641.
40. Kumagai K, et al. Effects of angiotensin II type 1 receptor antagonist on electrical and structural remodeling in atrial fibrillation. *J Am Coll Cardiol*. 2003;41(12):2197–2204.
41. Nattel S, Shiroshita-Takeshita A, Brundel BJ, Rivard L. Mechanisms of atrial fibrillation: lessons from animal models. *Prog Cardiovasc Dis*. 2005;48(1):9–28.
42. Suzuki M, et al. Functional roles of cardiac and vascular ATP-sensitive potassium channels clarified by Kir6.2-knockout mice. *Circ Res*. 2001;88(6):570–577.
43. Oka T, et al. Cardiac-specific deletion of Gata4 reveals its requirement for hypertrophy, compensation, and myocyte viability. *Circ Res*. 2006;98(6):837–845.
44. Jensen BM, Swindle EJ, Iwai S, Gilfillan AM. Generation, isolation, and maintenance of rodent mast cells and mast cell lines. In Coligan, JE, Bierer, B, Margulies, DH, Shevach, EM, Strober, W, Coico, R, eds. *Current Protocols in Immunology*. Hoboken, NJ: John Wiley & Sons; 2006:Chapter 3:Unit 3.23.
45. Zou Y, et al. Cell type-specific angiotensin II-evoked signal transduction pathways: critical roles of Gbetagamma subunit, Src family, and Ras in cardiac fibroblasts. *Circ Res*. 1998;82(3):337–345.
46. Takakura N, Yoshida H, Kunisada T, Nishikawa S, Nishikawa SI. Involvement of platelet-derived growth factor receptor-alpha in hair canal formation. *J Invest Dermatol*. 1996;107(5):770–777.